Kinetics and Mechanisms of Aqueous Ozone Reactions with Bromide, Sulfite, Hydrogen Sulfite, Iodide, and Nitrite Ions

Qian Liu, Lynn M. Schurter, Charles E. Muller, Simone Aloisio, Joseph S. Francisco, and Dale W. Margerum*

Department of Chemistry, Purdue University, West Lafayette, Indiana 47907-1393

Received August 11, 2000

Reactions of ozone with Br^-, SO_3^{2-}, HSO_3^-, I^-, and NO_2^-, studied by stopped-flow and pulsed-accelerated-flow techniques, are first order in the concentration of O_3(aq) and first order in the concentration of each anion. The rate constants increase by a factor of 5×10^6 as the nucleophilicities of the anions increase from Br^- to SO_3^{2-}. Ozone adducts with the nucleophiles are proposed as steady-state intermediates prior to oxygen atom transfer with release of O_2. Ab initio calculations show possible structures for the intermediates. The reaction between Br^- and O_3 is accelerated by H^+ but exhibits a kinetic saturation effect as the acidity increases. The kinetics indicate formation of $BrOOO^-$ as a steady-state intermediate with an acid-assisted step to give BrOH and O_2. Temperature dependencies of the reactions of Br^- and HSO_3^- with O_3 in acidic solutions are determined from 1 to 25 °C. These kinetics are important in studies of annual ozone depletion in the Arctic troposphere at polar sunrise.

Introduction

Ozone reacts rapidly with a wide range of inorganic ions in aqueous solution.[1] The kinetics of its reactions with bromide, sulfite, hydrogen sulfite, iodide, and nitrite are important in environmental studies and in water treatment processes.[2] The reaction of O_3 with Br^- is of great concern in ozonation processes because it is the first step leading to the generation of BrO_3^-. Bromate ion has been identified as a carcinogen and neurotoxin, and a maximum contamination level of 0.01 mg/L has been set by the US EPA.[3] In addition, the reactions of O_3 with Br^- and O_3 with S(IV) species are involved in the ozone depletion chemistry in the Arctic troposphere.[4] The kinetics of these reactions[5−8] are revisited with focus on the reactions at low pH and low temperature because of their possible role in reactions in Arctic aerosols, sea ice, and snowpack. The reaction of O_3 with I^- in seawater affects the global flux of iodine[9,10] and may be important in taste and odor problems in drinking water.[11] The reaction is very fast, and until now the rate constant has only been estimated.[10] Similarly, the reaction between O_3 and SO_3^{2-} is extremely rapid and the rate constant has been estimated from the S(IV) reactions from pH −0.30 to 4.02, where HSO_3^- and SO_2 are the main species present.[5] In the present work, pulsed-accelerated-flow (PAF) spectrometry[12,13] is used for the direct determination of the O_3 rate constants with I^- and SO_3^{2-}. The reaction of O_3 with NO_2^- is important both in water treatment processes and in atmospheric chemistry. The reaction kinetics were previously studied[1,9,14] only below pH 5. We use stopped-flow methods to extend the pH range from 1.5 to 10.6.

Comparison of the kinetics and rate constants for these five anions with O_3 leads to the proposal that adduct formation occurs followed by oxygen-atom transfer with the direct elimination of O_2. Ab initio calculations show feasible structures for the O_3−anion adducts.

Experimental Section

Reagents. Solutions of Br^-, I^-, SO_3^{2-}, HSO_3^-, and NO_2^- are prepared from their respective sodium salts immediately prior to use in pre-ozonated, freshly boiled, argon-purged water and are protected with argon until use. The water used to prepare the SO_3^{2-} and HSO_3^- solutions requires thorough argon purging (>1 h) to adequately remove oxygen and protect against S(IV) loss. Solution acidity is adjusted with standardized $HClO_4$, H_2SO_4, carbonate-free NaOH, and the following buffers: $HC_2H_3O_2$ ($pK_a = 4.41$[15] at $\mu = 0.50$ M, $pK_a = 4.26$[15] at $\mu = 0.10$ M), NaH_2PO_4 ($pK_a = 6.57$[16] at $\mu = 0.50$ M, $pK_a = 6.72$[16] at $\mu = 0.10$ M), and $NaHCO_3$ ($pK_a = 9.70$[12,17] at $\mu = 0.50$ M, $pK_a = 10.00$[18]

(1) Hoigné, J.; Bader, H.; Haag, W. R.; Staehelin, J. *Water Res.* **1985**, *19*, 993−1004.
(2) Hoigné, J. Chemistry of Aqueous Ozone and Transformation of Polluants by Ozonation. *Handbook of Enironmental Chemistry*; Hrubec, J., Ed.; Springer-Verlag: Berlin, 1998; Vol. 5, Part C, pp 83−141.
(3) US EPA. National Drinking Water Regulations: Disinfectants and Disinfection Byproducts. *Fed. Regist.* **1998**, *63*, 69390−69476.
(4) Oum, K. W.; Lakin, M. J.; Finlayson-Pitts, B. J. *Geophys. Res. Lett.* **1998**, *25*, 3923−3926.
(5) Erickson, R.; Yates, L.; Clark, R.; McEwen, D. *Atmos. Environ.* **1977**, *11*, 813−817.
(6) Haruta, K.; Takeyama, T. *J. Phys. Chem.* **1981**, *85*, 2382−2388.
(7) Haag, W. R.; Hoigné, J. *Environ. Sci. Technol.* **1983**, *17*, 261−267.
(8) Maahs, H. G. *Atmos. Environ.* **1983**, *17*, 341−345.
(9) Garland, J. A.; Curtis, H. *J. Geophys. Res.* **1981**, *86*, 3183−3186.
(10) Garland, J. A.; Elzerman, A. W.; Penkett, S. A. *J. Geophys. Res.* **1980**, *85*, 7488−7492.
(11) Bishel, Y.; von Guten, U. *Environ. Sci. Technol.* **1999**, *33*, 4040−4045.
(12) Fogelman, K. D.; Walker, D. M.; Margerum, D. W. *Inorg. Chem.* **1989**, *28*, 986−993.
(13) Bowers, C. P.; Fogelman, K. D.; Nagy, J. C.; Ridley, T. Y.; Wang, Y.; Evetts, S. W.; Margerum, D. W. *Anal. Chem.* **1997**, *69*, 341−438.
(14) Penkett, S. A. *Nature Phys. Sci.* **1972**, *240*, 105−106.
(15) Urbansky, E. T.; Cooper, B. T.; Margerum, D. W. *Inorg. Chem.* **1997**, *36*, 1338−1344.
(16) Smith, R. M.; Martell, A. E. *Critical Stability Constants*; Plenum: New York, 1976; Vol. 4.
(17) Odier, M.; Plichon, V. *Anal. Chim. Acta* **1971**, *55*, 209−220.
(18) Frydman, N.; Nilsson, G.; Rengemo, T.; Sillen, L. G. *Acta Chem. Scand.* **1958**, *12*, 878−884.

10.1021/ic000919j CCC: $20.00
Published on Web 07/19/2001

at $\mu = 0.10$ M). Solutions of $NaClO_4$ are prepared from the recrystallized solid and standardized gravimetrically for use in adjusting the ionic strength of all solutions. The pH measurements are taken shortly after the experiments are conducted, and the measured pH values are corrected to $p[H^+]$ ($=-\log[H^+]$) on the basis of electrode calibration data.

Generation of Ozone. Ozone is generated by passing research grade oxygen through a coaxial ozonator tube, which is powered by a 9 kV, 30 mA neon sign transformer. The molar absorptivity value for ozone in solution was reviewed by Maahs[8] and determined spectrophotometrically in this study to be 3000 M^{-1} cm^{-1} at 260 nm. The ozone/oxygen mixture is bubbled via gas dispersion tubes through acidic reaction solutions. The concentration of ozone in solution is measured immediately prior to use by a Perkin-Elmer Lambda 9 UV−vis spectrophotometer, and solutions are kept acidic under red light to minimize decomposition.

Kinetic Methods. Stopped-flow methods are used to measure O_3 reactions with Br^-, HSO_3^-, and NO_2^- under pseudo-first-order conditions with excess concentrations of these nucleophiles. Under these conditions, solvent decomposition of O_3 is negligible during the kinetic measurements. First-order conditions are advantageous, where possible, because the relative O_3 concentrations are measured during the reaction so that volatility is not a problem.

Data for NO_2^- reactions are collected by monitoring the disappearance of O_3 at 260 nm on a Dionex-Durrum Model D-110 stopped-flow spectrophotometer. Data for the reactions of O_3 with Br^- and HSO_3^- are collected on an Applied PhotoPhysics stopped-flow spectrophotometer, Model SX.18MV. The appearance of Br_3^- at 266 nm ($\epsilon_{Br_3^-} = 40\,900$ M^{-1} cm^{-1})[19] is monitored for the O_3 reaction with Br^-. The disappearance of O_3 at 260 nm is monitored for the reaction between O_3 and HSO_3^-.

Pseudo-first-order rate constants (k_{obsd}) are obtained from fits of $\ln(A_t - A_\infty)/(A_0 - A_\infty)$ vs time. Kinetic data are fit to the first-order model represented by eq 1, where $[X^{n-}] = [NO_2^-]$, $[Br^-]$, $[HSO_3^-]$ and k_{12} is

$$\frac{-d[O_3]}{dt} = k_{obsd}[O_3] \quad k_{obsd} = k_{12}[X^{n-}] \tag{1}$$

the second-order reaction rate constant. The reactions are followed for at least 5 half-lives. All kinetic traces are an average of 5 runs. Temperatures are controlled to ± 0.2 °C.

PAF methods are used to measure the extremely fast reactions of I^- and SO_3^{2-} with O_3 at 25.0 ± 0.2 °C. In these cases, second-order unequal-concentration conditions are necessary to obtain the rate constants. On the PAF Model IV instrument,[13] integrating observation over an optical path length of 2.05 cm during a 0.22 s pulse of continuous flow enables the collection of 250 points of intensity vs time data per trial. The solutions are mixed by employing a decelerated flow velocity of 12 to 3 m/s. The mixing constant (k_{mix}) in eq 2 is a

$$k_{mix} = k_m \upsilon \tag{2}$$

$$\frac{1}{k_{app}} = \frac{1}{k_m \upsilon} + \frac{1}{k_r} \tag{3}$$

function of the flow velocity (υ) and a proportionality constant (k_m). The apparent rate constant (k_{app}) is defined by the double-reciprocal relationship in eq 3, where k_r is the first-order reaction rate constant. For pseudo-first-order reaction conditions where k_{app} is greater than 4000 s^{-1}, eq 4 describes the relationship between absorbance and

$$M_{exptl} = \frac{A_\upsilon - A_\infty}{A_0 - A_\infty} = \frac{\upsilon}{bk_{app}} = \frac{1}{bk_m} + \frac{\upsilon}{bk_r} \tag{4}$$

velocity. M_{exptl} represents the degree of reaction in the observation path, A_υ is the absorbance at a particular solution velocity, A_0 is the initial absorbance of the reaction, A_∞ is the absorbance at infinite time, and b is the path length of the cell. The upper limit of PAF measurements is approached in acquiring data for the very fast reactions of O_3 with SO_3^{2-} and with I^- ions. Because of this fact, the reactions are run under second-order unequal-concentration conditions with O_3 as the limiting reactant. For irreversible second-order reaction conditions,[20] the second-order apparent rate constant is defined by the double-reciprocal relationship in eq 5, with M_{exptl} defined by eq 6, where $q = C_A/C_B$ ($C_A > C_B$). Iteration of eqs 6 and 7 yields $k_{12,app}$, and a plot of $1/k_{12,app}$ vs $1/\upsilon$ gives a slope of $1/k_{m,12}$ and an intercept of $1/k_{12}$ (reciprocal of the second-order rate constant for the reaction).

$$\frac{1}{k_{12,app}} = \frac{1}{k_{m,12}\upsilon} + \frac{1}{k_{12}} \tag{5}$$

$$M_{exptl} = \frac{A_v - A_A(1-q) - A_p}{A_A + (1/q)(A_B - A_p)} = \left(\frac{1-q}{R}\right)\ln\left(\frac{1-qe^{-R}}{1-q}\right) \tag{6}$$

$$R = \frac{bk_{12,app}C_A(1-q)}{\upsilon} \tag{7}$$

For faster reaction conditions, where $qe^{-R} \ll 1 (<0.05)$, the iteration on R can be eliminated and M_{exptl} is represented by eq 8. Substitution of eq 5 into eq 8 yields eq 9, which enables a direct calculation of k_{12} from the inverse of the slope of a plot of M_{exptl} vs υ.

$$M_{exptl} = \frac{A_\upsilon - A_\upsilon(1-q) - A_p}{A_\upsilon + (1/q)(A_B - A_p)} = \frac{\upsilon}{bk_{app}C_A}\ln\frac{1}{1-q} \tag{8}$$

$$M_{exptl} = \left(\frac{1}{k_{m,12}} + \frac{\upsilon}{k_{12}}\right)\frac{\ln[(1-q)^{-1}]}{C_A b} \tag{9}$$

It has been shown that reliable k_{12} values are obtained for second-order unequal conditions where the initial half-life, $t_{1/2}$, as defined by eq 10, is greater than 22 μs. Our smallest $t_{1/2}$ value is 26 μs.

$$(t_{1/2})_i = \frac{1}{k_{12}}\left(\frac{1}{C_A - C_B}\right)\ln\left(\frac{2C_A - C_B}{C_A}\right) \tag{10}$$

Computation. Calculations are performed using the GAUSSIAN 94[21] suite of programs to determine what are the plausible structures for the reaction intermediates. Equilibrium geometries are optimized using the Becke three-parameter hybrid functional combined with the Lee, Yang, and Parr correlation (B3LYP)[22] density functional theory method. This method is used with the 6-31G(d) basis set in the full optimization of the geometries. Harmonic vibrational frequencies are calculated at this level of theory to verify if the resulting structures are true minimums.

Results and Discussion

O_3 Reaction with Br^-. The reaction between O_3 and Br^- is followed under pseudo-first-order conditions with Br^- (0.50−100 mM) in large excess over O_3 ($\sim 10^{-5}$ M) at 25.0 ± 0.2 °C, $p[H^+] = 5.9$, and $\mu = 0.46$ M. Under conditions of excess Br^-, Br_3^- forms rapidly once Br^- is oxidized to Br_2. The rate of O_3

(19) Wang, T. X.; Kelley, M. D.; Cooper, J. N.; Beckwith, R. C.; Margerum, D. W. *Inorg. Chem.* **1994**, *33*, 5872−5878.

(20) Gerritsen, C. M.; Gazda, M.; Margerum, D. W. *Inorg. Chem.* **1993**, *32*, 5739−5748.

(21) Frisch, M. J.; Trucks, G. W.; Schlegel, H. B.; Gill, P. M. W.; Johnson, B. G.; Robb, M. A.; Cheeseman, J. R.; Keith, T.; Petersson, G. A.; Montgomery, J. A.; Raghavachari, K.; Al-Laham, M. A.; Zakrzewski, V. G.; Ortiz, J. V.; Foresman, J. B.; Cioslowski, J.; Stefanov, B. B.; Nanayakkara, A.; Challacombe, M.; Peng, C. Y.; Ayala, P. Y.; Chen, W.; Wong, M. W.; Andres, J. L.; Replogle, E. S.; Gomperts, R.; Martin, R. L.; Fox, D. J.; Binkley, J. S.; Defrees, D. J.; Baker, J.; Stewart, J. P.; Head-Gordon, M.; Gonzalez, C.; Pople, J. A. *Gaussian 94*, revision B.3; Gaussian, Inc.: Pittsburgh, PA, 1995.

(22) Becke, A. M. *J. Chem. Phys.* **1993**, *98*, 5648−5652.

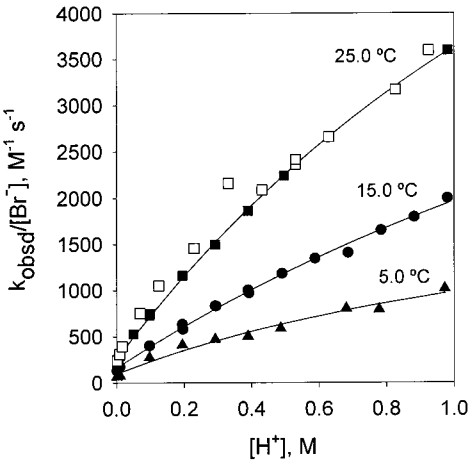

Figure 1. Temperature and $[H^+]$ dependence of the O_3 reaction with Br^-. Conditions: $[Br^-] = 100$ mM, $\mu = 1.0$ M ($NaClO_4$), acidity is adjusted with $HClO_4$, except for open squares, where H_2SO_4 is used.

loss (eq 1) equals the rate of $[Br_2]_T$ ($= [Br_2] + [Br_3^-]$) formation. Individual kinetic traces give excellent first-order fits in $[O_3]$. The plot of k_{obsd} vs $[Br^-]$ is linear, indicating a first-order dependence on $[Br^-]$. Linear regression of the data yields k_{12} equal to 248 ± 1 M^{-1} s^{-1} from the slope and an intercept (with a very small correction for O_3 loss in the absence of Br^-) statistically equal to zero.

The acid dependence study is carried out at 1.0 M ionic strength for $p[H^+] = 0-3$ with perchloric or sulfuric acid ($pK_a = 1.32$).[16] Sulfuric acid is chosen because of its high levels in Arctic aerosols and to test if HSO_4^- acts as a general acid to accelerate the reaction. Figure 1 shows both the $HClO_4$ results (black squares) and the H_2SO_4 results (open squares) at 25.0 °C. Four facts are evident: (1) the reaction rate is assisted by $[H^+]$; (2) the rate constants show evidence of a saturation effect as $[H^+]$ increases; (3) HSO_4^- does not accelerate the reaction as a general acid (the H_2SO_4 results are similar to the $HClO_4$ results); (4) the nonzero intercept is consistent with a water pathway.

Haruta and Takeyama[6] showed that $[H^+]$ assists the reaction; however, the $[H^+]$ dependence we find deviates greatly from the linear relationship they reported. Our study covers a much wider $[H^+]$ range (10^{-3} to 1.0 M) compared to their range of 10^{-3} to $10^{-1.2}$ M, and the second-order experimental conditions they used require accurate knowledge of the initial O_3 concentrations to calculate the rate constants.

On the basis of our kinetic data, a mechanism is proposed as shown in Scheme 1, where O_3 reacts with Br^- to form the steady-state intermediate $BrOOO^-$ in the first step. This intermediate subsequently reacts with H^+ or H_2O to give O_2 and HOBr.

Scheme 1

$$O_3 + Br^- \underset{k_{-1}}{\overset{k_1}{\rightleftharpoons}} BrOOO^-$$

$$BrOOO^- + H^+ \xrightarrow{k_2} HOBr + O_2$$

$$BrOOO^- + H_2O \xrightarrow{k_3} HOBr + O_2 + OH^-$$

$$HOBr + Br^- + H^+ \overset{\text{fast}}{\rightleftharpoons} Br_2 + H_2O$$

$$Br_2 + Br^- \overset{\text{fast}}{\rightleftharpoons} Br_3^-$$

Table 1. Parameters and Calculated Rate Constants for O_3 Reaction with Br^- at $\mu = 1.0$ M[a]

temp, °C	k_1, M^{-1} s^{-1}	k_2/k_{-1}, M^{-1}	k_3/k_{-1}	k_{H2O}, M^{-1} s^{-1}	k_{H+}, M^{-1} s^{-1}
25.0	1.10×10^4	0.47	0.024	2.58×10^2	3.64×10^3
15.0	7.59×10^3	0.33	0.022	1.63×10^2	1.99×10^3
5.0	2.41×10^3	0.64	0.042	97	9.77×10^2

[a] $\Delta H^{\ddagger}_{k1} = 50 \pm 10$ kJ/mol and $\Delta S^{\ddagger}_{k1} = 2 \pm 50$ J K^{-1} mol^{-1}. $\Delta H^{\ddagger}_{H^+} = 43.0 \pm 1.2$ kJ/mol and $\Delta S^{\ddagger}_{H^+} = -32 \pm 1$ J K^{-1} mol^{-1}, at 1.0 M $[H^+]$. $\Delta H^{\ddagger}_{H_2O} = 31.2 \pm 0.6$ kJ/mol and $\Delta S^{\ddagger}_{H_2O} = -94 \pm 2$ J K^{-1} mol^{-1}. k_1, k_2/k_{-1}, and k_3/k_{-1} values are determined by fitting the data to eq 11. k_{H_2O} values are calculated from eq 12, and k_{H^+} values are calculated from eq 11 at 1.0 M $[H^+]$.

The rate expression is derived in eq 11 based on a steady-state approximation in $[BrOOO^-]$. The water path rate constant (k_{H_2O}) (eq 12) is valid at very low $[H^+]$.

$$\frac{k_{obsd}}{[Br^-]} = \frac{k_1\left(\frac{k_2}{k_{-1}}[H^+] + \frac{k_3}{k_{-1}}\right)}{1 + \frac{k_2}{k_{-1}}[H^+] + \frac{k_3}{k_{-1}}} \tag{11}$$

$$k_{H_2O} = \frac{k_1}{\frac{k_{-1}}{k_3} + 1} \tag{12}$$

Experimental data collected at three temperatures (25.0, 15.0, and 5.0 °C) are fit with eq 11 using a nonlinear curve-fitting program with a Marquardt−Levenberg algorithm (SigmaPlot). As shown in Figure 1, the experimental results correspond to the proposed mechanism at all temperatures, showing strong support for the presence of a steady-state intermediate species. Three parameters (k_1, k_2/k_{-1}, and k_3/k_{-1}) are determined from the data at each temperature. Values for k_{H_2O} and for k_{H^+} ($= k_{obsd}/[Br^-]$ at $[H^+] = 1.0$ M) are summarized in Table 1. The k_{H_2O} value obtained in this $[H^+]$ dependence study is 258 $\pm$ 18 M^{-1} s^{-1} at 25.0 °C and $\mu = 1.0$ M, which is within experimental error of the value of 248 ± 1 M^{-1} s^{-1} ($\mu = 0.46$ M, 25.0 °C) obtained from the $[Br^-]$ dependence study. A small difference may be caused by the difference in ionic strength for the two cases. Both values are somewhat larger than the hydrogen-ion-independent path rate constant of 211 M^{-1} s^{-1} (27 °C, $\mu = 0.1$ M) reported by Haruta and Takeyama[6] and significantly larger than the value of 160 M^{-1} s^{-1} reported by Haag and Hoigné.[7]

Activation enthalpies and entropies are calculated (eq 13) for k_1, the water path, and the proton path from the data in Figure 1. The $\Delta H^{\ddagger}_{k1}$ value is 50 ± 10 kJ mol^{-1}, the proton path gives

$$\ln\left(\frac{k}{T}\right) = \ln\left(\frac{k_B}{h}\right) + \frac{\Delta S^{\ddagger}}{R} - \frac{\Delta H^{\ddagger}}{RT} \tag{13}$$

$\Delta H^{\ddagger}_{H^+} = 43.0 \pm 1.2$ kJ mol^{-1}, and the water path gives $\Delta H^{\ddagger}_{H_2O} = 31.2 \pm 0.6$ kJ mol^{-1}. The $\Delta S^{\ddagger}$ values are also given in Table 1. Under possible Arctic conditions at 273 K and 1.0 M acid, the predicted rate constants for Br^- reaction with O_3 is $k_{H^+} = 6.81 \times 10^2$ M^{-1} s^{-1}.

O_3 Reaction with SO_3^{2-}. S(IV) is distributed among SO_2 (aq), HSO_3^-, and SO_3^{2-} as a function of pH.[23] Erickson et al.[5] showed that O_3 reacts with S(IV) from $p[H^+] = -0.30$ to 4.02 with a first-order dependence in $[O_3]$ and a first-order depen-

(23) Brandt, C.; van Eldik, R. *Chem. Rev.* **1995**, *95*, 119−190.

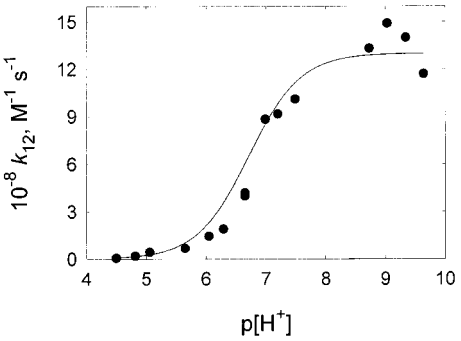

Figure 2. p[H$^+$] dependence of the O_3 reaction with SO_3^{2-}. Conditions: initial $[O_3] = (2.46-3.89) \times 10^{-5}$ M, initial $[SO_3^{2-}]_T = 3.00 \times 10^{-5}$ to 3.00×10^{-4} M, $\mu = 0.1$ M, 25.0 °C, [acetate]$_T$ = 10 mM for p[H$^+$] = 4.5−5.06, [phosphate]$_T$ = 10 mM for p[H$^+$] = 5.65−7.49, [carbonate]$_T$ = 20 mM for p[H$^+$] = 8.73−9.64.

dence in S(IV). The kinetic contribution of SO_2 was not evaluated, but it was negligible above pH 2.

In the present work, the kinetics of the O_3/S(IV) reaction are investigated at p[H$^+$] = 4.50−9.64 at 25.0 ± 0.2 °C and μ = 0.10 M, with $[O_3] = (2.46-3.89) \times 10^{-5}$ M and $[SO_3^{2-}]_T = 3.00 \times 10^{-5}$ to 3.00×10^{-4} M. In this p[H$^+$] range, the concentration of SO_2(aq) is negligible (pK_{a1} = 1.90, pK_{a2} = 6.30)[23] and the experimental rate constant k_{12} due to SO_3^{2-} and HSO_3^- is expressed by eq 14. The experimental second-order

$$k_{12} = \frac{k_{SO_3^{2-}} K_{a2} + k_{HSO_3^-}[H^+]}{K_{a2} + [H^+]} \qquad (14)$$

rate constants obtained from eqs 5−7 are plotted as a function of [H$^+$] in Figure 2. A nonlinear curve fit of the data using eq 14 yields a value of $(1.3 \pm 0.1) \times 10^9$ M^{-1} s^{-1} for $k_{SO_3^{2-}}$ with a negligible HSO_3^- contribution (i.e., $k_{HSO_3^-}$ is less than 10^6 M^{-1} s^{-1}). The rate constant for SO_3^{2-} with O_3 agrees with the value of 1.0×10^9 M^{-1} s^{-1} at 22 °C obtained from data extrapolated from pH 5.2.[1]

Our value for $k_{SO_3^{2-}}$ is significantly smaller than the value of 2.2×10^9 M^{-1} s^{-1} reported by Erickson et al.[5] They studied this reaction below pH 4.02, where the HSO_3^- species is dominant and the kinetics of HSO_3^- and SO_3^{2-} reactions with O_3 both contribute. In our study, the p[H$^+$] range (4.50−9.64) is chosen such that the SO_3^{2-} reaction with O_3 is the dominant path and its rate constant is more accurately evaluated. The disagreement in $k_{SO_3^{2-}}$ values may also be attributable to the difference in ionic strength, which is controlled at 0.10 M in our study, whereas the ionic strength was not mentioned in the previous studies.[1,5]

O_3 Reaction with HSO_3^-. We also studied the kinetics of the O_3 reaction with S(IV) under more acidic conditions (p[H$^+$] = 0.49−1.20) by stopped-flow spectroscopy under pseudo-first-order conditions with $[HSO_3^-]_T$ (from 0.48 to 2.97 mM) in large excess over O_3 (~10^{-5} M) and μ = 1.0 M. In this p[H$^+$] range, SO_2(aq) and HSO_3^- are the major forms of S(IV) while the SO_3^{2-} concentration is very low. However, the value of $k_{SO_3^{2-}}$ is so large that SO_3^{2-} may still make a small contribution to the observed reaction rate. Equation 15 gives the rate expression,

$$\frac{k_{obsd}}{[S(IV)]_T} = \frac{k_{SO_3^{2-}} K_{a1} K_{a2} + k_{HSO_3^-} K_{a1}[H^+] + k_{SO_2}[H^+]^2}{K_{a1}K_{a2} + K_{a1}[H^+] + [H^+]^2} \qquad (15)$$

taking into consideration the contributions of all three species. Figure 3 shows the results of the $[S(IV)]_T$ dependence study at

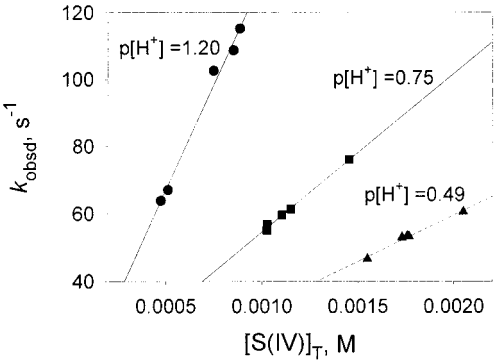

Figure 3. $[S(IV)]_T$ dependence of the O_3 reaction with HSO_3^-. Conditions: $[O_3] = \sim 10^{-5}$ M, $[HSO_3^-]_T = 0.48-2.97$ mM, μ = 1.0 M, 25.0 °C, acidity is adjusted with $HClO_4$.

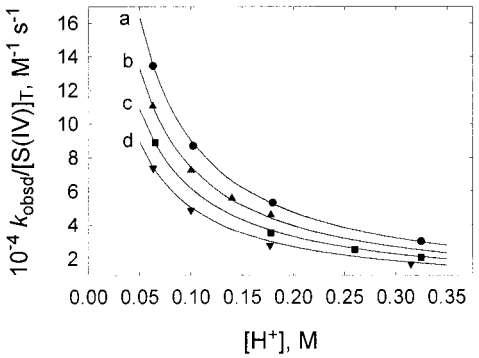

Figure 4. Temperature and [H$^+$] dependence of the O_3 reaction with HSO_3^-. Conditions: μ = 1.0 M, acidity is adjusted with $HClO_4$.

25 °C and p[H$^+$] values of 0.49, 0.75, and 1.20. The reaction is first order in $[S(IV)]_T$ at all p[H$^+$] values. Figure 4 shows the result of the [H$^+$] dependence study for [H$^+$] = 0.05−0.35 M at four temperatures. At μ = 1.0 M, pK_{a1} values of 1.90, 1.79, 1.71, and 1.63 are used for 25.0, 15.0, 8.1, and 1.2 °C, respectively, based on $\Delta H° = -18$ kJ mol^{-1}.[24] For the same temperatures and ionic strength values the respective pK_{a2} values are 6.30, 6.15, 6.06, and 5.96, based on $\Delta H° = -12.3$ kJ mol^{-1}.[25] At 25.0 °C the $k_{SO_3^{2-}}$ value of 1.3×10^9 M^{-1} s^{-1} is used in the fit of data to eq 15, which yields $k_{HSO_3^-} = (8.0 \pm 0.1) \times 10^5$ M^{-1} s^{-1} at μ = 1.0 M and a k_{SO_2} value that is statistically equal to zero. Hoigné et al.[1] reported a value of 3.2×10^5 M^{-1} s^{-1} at 22 °C based on the same pK_1 value but with a pK_{a2} value of 7.2. The ionic strength was not given. The contribution of the SO_3^{2-} path to the overall rate is only 1.3% at p[H$^+$] = 1.20 and 0.3% at p[H$^+$] = 0.49 at 25.0 °C. At lower temperatures, measurements at the highest acidity are used to evaluate $k_{HSO_3^-}$ by first neglecting the contributions of SO_3^{2-}. This yields $k_{HSO_3^-} = (5.6 \pm 0.2) \times 10^5$ M^{-1} s^{-1} at 15.0 °C, $(3.6 \pm 0.2) \times 10^5$ M^{-1} s^{-1} at 8.1 °C, and $(2.43 \pm 0.04) \times 10^5$ M^{-1} s^{-1} at 1.2 °C. These values are almost the same as the values of $k_{HSO_3^-} = (5.23 \pm 0.03) \times 10^5$ M^{-1} s^{-1} at 15.0 °C, $(3.69 \pm 0.05) \times 10^5$ M^{-1} s^{-1} at 8.1 °C, and $(2.51 \pm 0.05) \times 10^5$ M^{-1} s^{-1} at 1.2 °C obtained when the 25 °C value of $k_{SO_3^{2-}}$ is used to fit all the temperature data. The latter gives the best fit of data (Figure 4), which indicates that the temperature dependence of $k_{SO_3^{2-}}$ is small. The values of $k_{SO_3^{2-}}$ as a function of temperature are not measured because the PAF Model IV instrument does not permit temperature variation.

(24) van Eldik, R.; Harris, G. *Inorg. Chem.* **1980**, *19*, 880−886.
(25) Sillén, L.; Martell, A. *Stability Constants of Metal Ion Complexes*; Burlington House: London, 1971; Supplement 1.

Table 2. Comparison of Experimental Rate Constants (25.0 °C, in M^{-1} s^{-1}) of the Reactions between Inorganic Ions (X^{n-}) with O_3 and $^{\bullet}CO_3^-$ with Predictions Based on a Marcus Outer-Sphere Electron-Transfer Model

			$O_3 + X^{n-}$		$^{\bullet}CO_3^- + X^{n-}$	
couple	$E°$, V	k_{11}	$k_{12,pred}$	$k_{12,obsd}$	$k_{12,pred}$	$k_{12,obsd}$
O_3/O_3^-	1.01[a]	4[b]				
$^{\bullet}CO_3^-/CO_3^{2-}$	1.59[c]	1.6[b]				
I/I^-	1.33[a]	2×10^8 [b]	29.1	1.2×10^9	1.9×10^6	2.5×10^8 [c]
NO_2/NO_2^-	1.04[a]	0.3[b]	0.061	5.83×10^5	1.0×10^4	6.6×10^5 [c]
$^{\bullet}SO_3^-/SO_3^{2-}$	0.72[d]	4[b]	1.3×10^3	1.3×10^9	9.2×10^6	2.9×10^7 [c]
$HSO_3^{\bullet}/HSO_3^-$				8.0×10^5		
Br/Br^-	1.92[a]			248		

[a] Reference 34. [b] Reference 28. [c] References 32 and 33. [d] Sarala, R.; Islam, M. A.; Rabin, S. B.; Stanbury, D. M. *Inorg. Chem.* **1990**, *29*, 1133−1142.

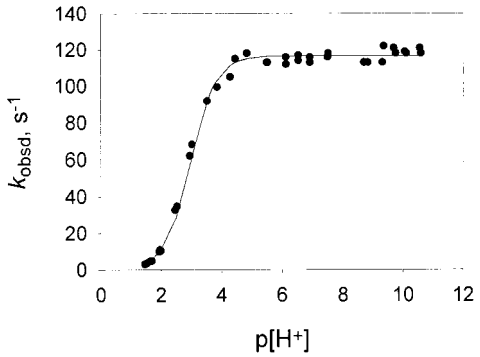

Figure 5. $[H^+]$ dependence of the reaction of O_3 with NO_2^-. Conditions: $[O_3] = (1.75-4.64) \times 10^{-5}$ M, $[NO_2]_T = 0.2$ mM, $\mu = 0.50$ M, 25.0 °C, no buffer for $p[H^+] = 1.46-3.02$, acetate buffer for $p[H^+] = 3.52-4.83$, phosphate buffer for $p[H^+] = 5.49-7.52$, carbonate buffer for $p[H^+] = 8.72-10.61$, $[buffer]_T = 0.050$ M for all buffers.

The activation enthalpy and entropy for the HSO_3^- reaction with O_3, obtained from an Eyring plot (eq 13), give $\Delta H^{\ddagger}_{HSO_3^-} = 30.9 \pm 0.9$ kJ mol^{-1} and $\Delta S^{\ddagger}_{HSO_3^-} = -28 \pm 3$ J K^{-1} mol^{-1}. Much higher values were reported by Erickson et al.[5] from studies at only two temperatures (25 and 16 °C).

O_3 Reaction with I^-. The PAF method is used to study the reaction of O_3 with I^- at 25.0 °C by following the loss of O_3 at 260 nm under second-order unequal-concentration conditions ($[O_3] = (2.74-4.07) \times 10^{-5}$ M, $[I^-] = 3.34 \times 10^{-5}$ to 5.57×10^{-4} M, $p[H^+] = 6.7$, and $\mu = 0.1$ M). The average rate constant is $(1.2 \pm 0.1) \times 10^9$ M^{-1} s^{-1}. This is 240 times larger than the previously specified lower limit from direct chemical studies but agrees with a value of 1×10^9 M^{-1} s^{-1} estimated from surface deposition measurements.[10]

O_3 Reaction with NO_2^-. A nitrite dependence study is carried out at $p[H^+] = 2.0$, $\mu = 0.50$ M, and 25.0 °C with $[NO_2^-]$ in 10-fold excess over $[O_3]_{initial}$. Values of k_{obsd} show a first-order dependence in $[NO_2^-]$ with a second-order rate constant of $(6.08 \pm 0.06) \times 10^5$ M^{-1} s^{-1}. The reaction is also studied for $p[H^+] = 1.46-10.61$ under pseudo-first-order conditions. Figure 5 shows the $p[H^+]$ dependence of k_{obsd}. For $p[H^+] = 1.46-3.02$ there is no added buffer, but acetate, phosphate, and carbonate buffers are used to study the reaction for $p[H^+] = 3.5-10.6$. The studies show that the reactions have no buffer dependence.

There is an equilibrium between HNO_2 and NO_2^- with $pK_a = 2.97$ for HNO_2 at 25.0 °C and $\mu = 0.50$ M.[26] Equation 16 is

$$k_{obsd} = k_{12}\frac{K_a[NO_2^-]_T}{K_a + [H^+]} \qquad (16)$$

the expression for the observed rate constant, assuming that NO_2^- is the only reactive form. This gives an excellent fit of the data (Figure 5), with a second-order rate constant of $(5.83 \pm 0.04) \times 10^5$ M^{-1} s^{-1}, which is in reasonable agreement with the value obtained at $p[H^+] = 2$. Both rate constants are higher than previous values[1,2] which were obtained at either lower pH (pH 4)[9] at 25 °C or in a relatively narrow pH range (from 1.8 to 5)[1] at temperatures around 20−23 °C and then extrapolated to high pH.

Lack of General Acid−Base Effects. Previous studies of the kinetics of Br^- oxidation by HOBr[27] and of SO_3^{2-} oxidation by HOCl[12] have shown the importance of general-acid assistance in these halogen−cation transfer mechanisms. The O_3 oxidation of Br^-, NO_2^- and SO_3^{2-} are affected by the acidity of the solutions but not by buffer concentrations.

Conclusions

Mechanistic Comparisons. Table 2 compares the experimentally determined rate constants for the reactions of O_3 with I^-, NO_2^-, and SO_3^{2-} with values predicted from a Marcus outer-sphere electron-transfer mechanism. Values of the self-exchange rate constants for O_3/O_3^-, I/I^-, NO_2/NO_2^-, and SO_3^-/SO_3^{2-} are taken from Stanbury's review.[28] In these O_3 reactions, the experimental values ($k_{12,obsd}$) are many orders of magnitude greater than the predicted k_{12} values. For example, the $k_{12,obsd}$ value for the O_3/I^- reaction is so large that electron transfer can be ruled out because it would require the reverse reaction to be vastly greater than the diffusion-controlled rate. As Stanbury[29−30] and Bennett[31] have pointed out, reactions between main-group species rarely proceed by an outer-sphere electron-transfer mechanism. Greater orbital overlap can occur with nonmetal species than when one reactant is a metal ion shielded by ligands. They propose that greater orbital overlap can lead to a lower energy transition state. Table 2 gives rate constants from the work of Huie et al.[32−33] for the reactions of the carbonate radical ion ($^{\bullet}CO_3^-$), with I^-, NO_2^-, and SO_3^{2-}. The $^{\bullet}CO_3^-$ ion, generated by pulse radiolysis, is an even stronger one-electron oxidizing agent ($E° = 1.59$ V[33]) than is ozone ($E° = 1.01$ V[31]). The predicted outer-sphere electron-transfer rate

(26) Tummavuori, J.; Lumme, P. *Acta Chem. Scand.* **1968**, *22*, 2003−2011.

(27) Beckwith, R. C.; Wang, T. X.; Margerum, D. W. *Inorg. Chem.* **1996**, *35*, 995−1000.

(28) Stanbury, D. M. *Electron-Transfer Reactions*; Advances in Chemistry Series; American Chemical Society: Washington, DC, 1997; pp 165−182.

(29) Stanbury, D. M.; de Maine, M. M.; Goodloe, G. *J. Am. Chem. Soc.* **1989**, *111*, 5496−5498.

(30) Stanbury, D. M.; Martinez, R.; Tseng, E.; Miller, C. E. *Inorg. Chem.* **1988**, *27*, 4277−4280.

(31) Bennett, L. E.; Warlop, P. *Inorg. Chem.* **1990**, *29*, 1975−1981.

(32) Huie, R. E.; Neta, P.; Ross, A. B. *J. Phys. Chem. Ref. Data* **1988**, *17*, No. 3.

(33) Huie, R. E.; Shoute, L. C. T.; Neta, P. *Int. J. Chem. Kinet.* **1991**, *23*, 541−552.

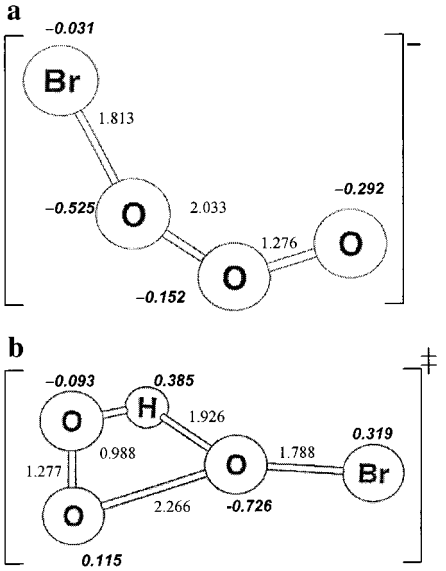

Figure 6. (a) Structure of the proposed $BrOOO^-$ intermediate from ab initio calculations with bond distances in Å. Values of the charge density are given in boldface and italic type. (b) Structure of the proposed transition state $[HOOOBr]^‡$ for the proton-assisted path.

constants are much larger than those for ozone, but the $k_{12,obsd}$ values for $^•CO_3^-$ with I^- and SO_3^{2-} are factors of 5 and 45 smaller, respectively, than the $k_{12,obsd}$ values for O_3. The $k_{12,obsd}$ values for the $^•CO_3^-$ oxidations are larger than the $k_{12,pred}$ values, but only by factors of 130 (for I^-), 66 (for NO_2^-) and 2.9 (for SO_3^{2-}). This suggests that weak interactions (orbital overlap) may occur between these anions and $^•CO_3^-$, whereas much stronger interactions occur with O_3.

We propose that with O_3 these nucleophiles form Lewis acid−base adducts as kinetic intermediates before the transition state. We also propose that these adducts react by oxygen-atom transfer rather than by electron transfer. Hoigné has also suggested oxygen-atom transfer reactions for NO_2^-, I^-, and Br^- reactions with O_3.[2] Our kinetic data require a $BrOOO^-$ intermediate in the reaction of Br^- with O_3. Ab initio calculations show that $BrOOO^-$ intermediates are possible. There are two minimum energy conformations for the $BrOOO^-$ intermediate. In one Br^- is weakly bound to O_3, and in the other a stronger Br−O bond forms at the expense of lengthening one of the O−O bonds in O_3 (Figure 6a). The calculations also show that both the proton path and the water path could go through a common transition state, as shown in Figure 6b, that leads to the elimination of residual O_2 and formation of HOBr. Aqueous solvation will undoubtedly have a large effect on the stability and reactivity of the intermediate; however, the calculated structures serve as useful models for the mechanism.

It is instructive to compare the energetics of atom-transfer vs electron-transfer for an intermediate such as $BrOOO^-$ (eqs 17 and 18). In aqueous solutions, reaction 17 is preferred over

$$BrOOO^- \rightarrow BrO^- + O_2 \text{ (atom transfer)} \qquad (17)$$

$$BrOOO^- \rightarrow Br^• + O_3^- \text{ (electron transfer)} \qquad (18)$$

reaction 18 by 402 kJ mol^{-1} (calculated from $E°$ values[34,35]). Hence, atom transfer is the overwhelmingly favorable path.

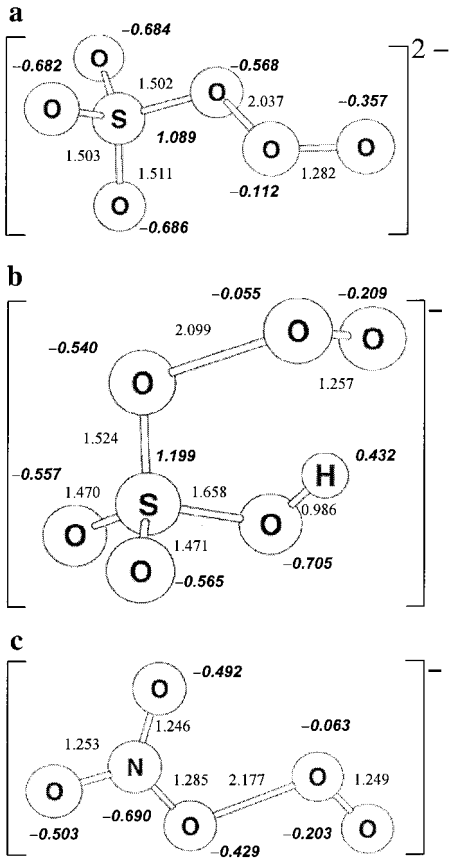

Figure 7. Structures of $O_3 \cdot X^{n-}$ adducts from ab initio calculations with bond distances in Å. Values of the charge density are given in boldface and italic type.

Table 3. Nucleophilicity (n) for Inorganic Anions (X^{n-}) and ΔH_{adduct} Values Calculated for $O_3 \cdot X^{n-}$

X^{n-}	n	ΔH_{adduct}, kJ mol^{-1} [c]
I^-	5.04[a]	
NO_2^-	4.2[b]	−225.5
SO_3^{2-}	5.10[a]	−487.9
HSO_3^-		−259.8
Br^-	3.89[a]	−2.9

[a] Swain, C. G.; Scott, C. B. *J. Am. Chem. Soc.* **1953**, *75*, 141. [b] Margerum, D. W.; Schurter, L. M.; Hobson, J.; Moore, E. E. *Environ. Sci. Technol.* **1994**, *28*, 331−337. [c] This work.

Results from ab initio calculations are consistent with this conclusion. In fact, the ab initio results suggest that the electron transfer (eq 18) is very endothermic, while the atom transfer (eq 17) is exothermic.

Structural changes during adduct formation also suggest that atom transfer is more favorable. Ab initio calculations yield structures of the intermediate adducts, as shown in Figures 6 and 7. The $(BrOOO)^-$ intermediate in Figure 6a has greatly lengthened one of the original O−O bonds in O_3, and its cleavage will give BrO^- and O_2. The H^+-assisted transition state in Figure 6b again shows that this bond is greatly elongated. Similarly by breaking the longest O−O bond, the $(O_3SOOO)^{2-}$ intermediate in Figure 7a, the $(HOSO_2OOO)^-$ intermediate in Figure 7b, and the $(O_2NOOO)^-$ intermediate in Figure 7c are poised to easily release O_2 and SO_4^{2-}, $HOSO_3^-$, and NO_3^-, respectively. With such structural changes, it is difficult for electron transfer to occur because more energy is required to break the already formed X−O bond (X = Br, S, N) and to readjust the two O−O bond lengths to form O_3^-.

(34) Stanbury, D. M. *Advances in Inorganic Chemistry*; Academic: New York, 1989; Vol. 33, pp 69−138.
(35) Bard, A. J.; Parsons, R.; Jordan, J. *Standard Potentials in Aqueous Solution*; Marcel Dekker: New York, 1985.

Nucleophilicity and ΔH_{adduct} Correlation. If the reactions of O_3 with NO_2^-, HSO_3^-, SO_3^{2-}, I^-, and Br^- all proceed via the same oxygen atom transfer mechanism, then the rate constant of these reactions should correlate with the nucleophilic reactivities of NO_2^-, HSO_3^-, SO_3^{2-}, I^-, and Br^- (Table 3) in accord with the Swain-Scott relationship (eq 19). In this equation

$$\log k_{12} = sn + b \tag{19}$$

n is the nucleophilicity of the anions and *s* is the sensitivity of the reaction rate constant to the strength of the nucleophile. Figure 8 includes a Swain−Scott plot of log k_{12} vs *n*. The dashed line is the linear regression through the data points (open squares) with NO_2^-, HSO_3^-, SO_3^{2-}, I^-, and Br^- on or near the line. The correlation supports an atom-transfer mechanism for these reactions. The slope of the plot gives $s = 5.1$ and shows that the ozone reaction is very sensitive to the nucleophilicity of the anion.

Also included in Figure 8 is a plot of log *k* vs $-\Delta H_{adduct}$. ΔH_{adduct} is the heat of formation (from ab initio calculations) for the adduct formed from O_3 and the nucleophiles (Table 3). The heat of formation of the adduct reflects the ability of the nucleophiles to donate an electron pair to O_3. The more negative ΔH_{adduct}, the stronger the interaction. An excellent correlation is found between ΔH_{adduct} and the reaction rate constant for each of the species. The solid line is the linear regression through the data points (black circles). It matches very well with the Swain−Scott nucleophilicity correlation plot. Both plots support adduct formation and an oxygen atom transfer mechanism.

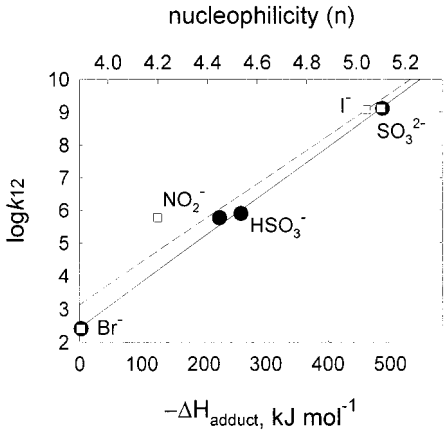

Figure 8. Swain−Scott nucleophilicity correlation (open squares and dashed line) and ΔH_{adduct} correlation (black circles and solid line) plots.

Acknowledgment. This work was supported by National Science Foundation Grants ATM-9631572, CHE-9818214, and CHE-9622683. We thank David Littlejohn (Lawrence Berkeley Laboratory) for help in initiating these studies.

Supporting Information Available: Tables and figures giving kinetic data. This material is available free of charge via the Internet at http://pubs.acs.org.

IC000919J